H MODE CONFINEMENT IN ALCATOR C-MOD

M. GREENWALD, R.L. BOIVIN, F. BOMBARDA[a], P.T. BONOLI, C.L. FIORE, D. GARNIER, J.A. GOETZ, S.N. GOLOVATO, M.A. GRAF, R.S. GRANETZ, S. HORNE, A. HUBBARD, I.H. HUTCHINSON, J.H. IRBY, B. LaBOMBARD, B. LIPSCHULTZ, E.S. MARMAR, M.J. MAY[b], G.M. McCRACKEN*, P. O'SHEA, J.E. RICE, J. SCHACHTER, J.A. SNIPES, P.C. STEK, Y. TAKASE, J.L. TERRY, Y. WANG, R. WATTERSON, B. WELCH[c], S.M. WOLFE
Plasma Fusion Center,
Massachusetts Institute of Technology,
Cambridge, Massachusetts,
United States of America

[a] Associazione Euratom–ENEA sulla Fusione, Frascati, Italy
[b] The Johns Hopkins University, Baltimore, Maryland, United States of America
[c] Institute for Plasma Research, University of Maryland, College Park, Maryland, United States of America

ABSTRACT. A series of experiments, examining the confinement properties of ion cyclotron range of frequencies (ICRF) heated H mode plasmas, has been carried out on the Alcator C-Mod tokamak. Alcator C-Mod is a compact tokamak that operates at high particle, power and current densities at toroidal fields up to 8 T. Under these conditions the plasma is essentially thermal with very little contribution to the stored energy from energetic ions (typically no more than 5%) and with $T_i \sim T_e$. Most of the data were taken with the machine in a single null 'closed' divertor configuration with the plasma facing components clad in molybdenum tiles. The data include those taken both before and after the first wall surfaces were coated with boron, with emphasis on the latter. H modes obtained from plasmas run on boronized walls typically had a lower impurity content and radiated power and attained a higher stored energy than those run on bare molybdenum. Confinement enhancement, the energy confinement time normalized to L mode scaling, for discharges with boronized walls, ranged from 1.6 to 2.4. The unique operating regime of the Alcator C-Mod device provided a means for extending the tests of global scaling laws to parameter ranges not previously accessible. For example, the Alcator C-Mod edge localized mode (ELM)-free data were found to be 1.1 to 1.6 times the ITERH93 scaling and the ELMy data almost 2.0 to 2.8 times the ITERH92 ELMy scaling law, suggesting that the size scaling in both scalings may be too strong. While both ELM-free and ELMy discharges were produced, the ELM characteristics were not easily compared with observations on other devices. No large, low frequency ELMs were seen despite the very high edge pressure and temperature gradients that were attained. For all of our H mode discharges, a clear linear relationship between the edge temperature pedestal and the temperature gradient in the core plasma was observed; the discharges with the 'best' transport barriers also showing the greatest improvement in core confinement. A summary of the data described is now available in the ITER H mode database.

1. INTRODUCTION

Alcator C-Mod (hereafter referred to as C-Mod) is a compact high field tokamak with a highly closed divertor and with capabilities for strong plasma shaping [1]. Its major radius is 0.68 m, its minor radius is 0.22 and its toroidal field, B_T, has been operated from 2.6 to 8.0 T. The plasma current, I_p, for these studies ranged from approximately 0.8 to 1.2 MA. Typical plasma elongations are in the range 1.6 to 1.75. The plasmas are somewhat 'D' shaped though, at the present time, the divertor geometry holds the lower triangularity to values in the range 0.5 to 0.6. Upper triangularity is typically 0.3 to 0.4. The plasma line averaged density, n_e, ranged from 1.3 to 4.3 $\times$ 10^{20} m^{-3}, with the better H modes all above 2 $\times$ 10^{20}. The auxiliary heating method is ion cyclotron range of frequencies (ICRF) heating; employing a hydrogen minority in deuterium plasmas at B_T = 5.3 T as the principal scenario. For these experiments, up to 3.5 MW of RF power were

* *Present address:* JET Joint Undertaking, Abingdon, Oxfordshire, United Kingdom.

available. Because of the large B/R ratio in C-Mod, ohmic heating is never negligible, contributing 0.5 to 1.5 MW depending on plasma temperature and purity. The first wall is composed of molybdenum tiles and is designed to take the very high power loadings that occur in this experiment; values for the parallel heat flux of up to 0.5 GW/m^2 have been measured [2]. The C-Mod divertor geometry, combined with the high densities, results in very effective baffling of neutrals. Divertor compression, the ratio of neutral pressure in the divertor chamber to the pressure in the main plasma chamber, ranges from 100 to 300 [3].

H modes are easily obtained in C-Mod with ohmic and RF heating, over a wide range in L mode target conditions, including densities up to 3×10^{20} m^{-3} and fields up to 8 T [4]. The power required for the L–H transition is consistent with $P_{tot}/S = 0.02 - -0.04\ nB_T$; with P_{tot}, the total input power measured in megawatts, S the plasma surface area in m^2, n_e in 10^{20} m^{-3} and B_T in teslas. The factors that cause the variation in required input power are not well understood, but seem to be related to impurity levels, wall conditioning and neutral pressure. Initially, the H modes were characterized by strong, high frequency edge localized modes (ELMs) or brief ELM-free periods with accumulating impurities and high ratios of $f_{rad} = P_{rad}/P_{tot}$. These results, combined with those reported on other devices [5], led us to study the effect of boronizing the vacuum chamber [6]. In C-Mod, vessel conditioning is accomplished via electron cyclotron discharge cleaning (ECDC) in which 2.5 kW of microwave power at 2.45 GHz is applied as the toroidal field is slowly ramped from 0.06 to 0.14 T (measured at R = 0.67 m), sweeping the resonance over the vacuum wall. For boronization, the discharge cleaning gas was replaced with a 9:1 mixture of helium and diborane (B_2D_6). The boron coating was renewed about once a week. Following boronization, radiated power, which was primarily due to molybdenum, was lower and H mode performance was dramatically improved. Unless explicitly stated, results in this paper refer to discharges produced following the boronization campaign.

2. MEASUREMENTS AND METHODOLOGY

The set of diagnostics available for transport studies on C-Mod includes: electron cyclotron emission (ECE) and Thomson scattering for measuring $T_e(r, t)$; a two colour interferometer (TCI), reflectometry and Thomson scattering for determining $n_e(r, t)$; an array of high resolution X ray spectrometers for measuring $T_i(r, t)$; neutron emission diagnostics for determining $T_i(0, t)$; a visible bremsstrahlung array for measuring $Z_{eff}(r, t)$; a bolometer array for measuring radiated power profiles, $P_{rad}(r, t)$; various spectrometers for determining impurity content; and a full set of magnetic diagnostics for calculating the magnetohydrodynamic (MHD) equilibrium and related quantities. The plasma stored energy is calculated by integration of the density and temperature profiles (W_{kin}) and by analysis of the equilibrium with the EFIT code [7] (W_{MHD}). These generally agree to within 20%. Most of this discrepancy can be understood as the result of errors in experimentally measured quantities; estimates of these errors are summarized in Table I. A residual systematic difference between the magnetic and kinetic calculations remains. The larger part of this difference can be explained as kinetic energy stored in the minority ion tail, leaving a residual systematic difference of less than 5% of the total. When suitable background data are available for subtraction of stray field effects, we can also obtain the stored energy by analysis of the diamagnetic loop signals. These are in good agreement with W_{MHD}. Shots for confinement analysis were chosen to be in quasi-steady state with respect to stored energy, density and magnetic equilibrium. Time slices used for comparison with scaling laws were chosen with $f_{rad} < 0.5$; $dW/dt < 0.35P_{in}$; $dn_e/dt < 0.4n_e/\tau_E$; and $q_{95} > 3$. (The selection criteria correspond to those of Refs [8, 9].)

Table I. Estimated Errors of Various Measured and Calculated Quantities

Measured quantity	Estimated error
I_p	3 kA
B_T	0.03 T
β_p	0.05–0.1
W_{MHD}	10–15 kJ
	5–10%
n_e	5–10%
T_e	10%
T_i	10–20%
W_{kin}	20%
P_{rad}	15–20%
P_{ICRF}	10%

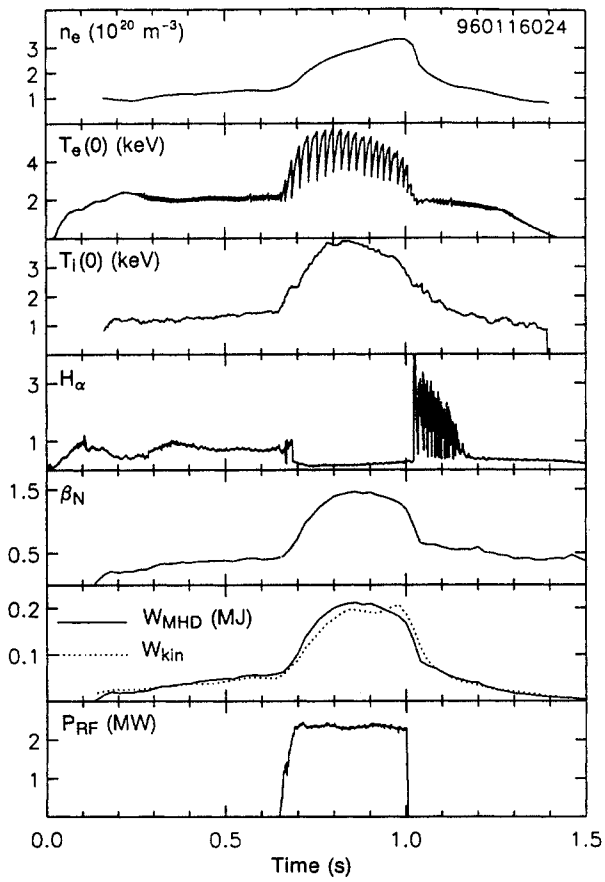

FIG. 1. Traces from an ELM-free H mode discharge, shot number 960116024. The plasma current was 1 MA and the toroidal field was 5.3 T.

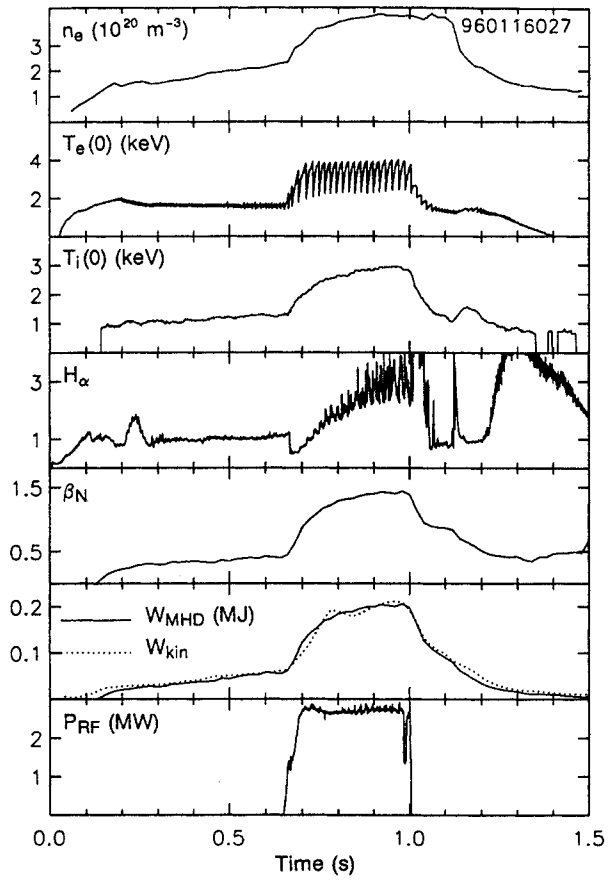

Fig. 2(a). Traces from an ELMy H mode, shot number 960116027. The current and field were the same as those for the shot in Fig. 1.

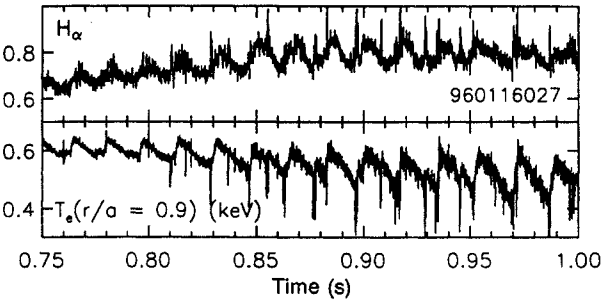

Fig. 2(b). Same discharge as that in Fig. 2(a), but with an expanded time-scale showing ELMs.

For full profile and time dependent analysis the TRANSP [10] code is used. This code uses measured plasma profiles as inputs and then calculates the electron and ion heat balance, the particle balance and the magnetic diffusion with a fixed boundary equilibrium. For ICRF heated plasmas, the full wave SPRUCE [11] code linked to the Fokker–Planck solver FPPRF [12] is used to calculate the heating power to ions and electrons. SPRUCE assumes perfect wave power absorption, and thus overestimates absorbed power. From an analysis of transients of RF perturbations (by changes in the slope of W_{dia}), we estimate the absorbed fraction to be $90 \pm 10\%$ and this number is used for all global calculations. For our H modes, which are at high densities, the code results indicate that the energy in fast ions is less than 5%. The 'thermal' nature of these plasmas is confirmed by observation of sawtooth reheat rates, which show very little contribution to plasma heating from fast ions immediately following the turn-off of ICRF power. For similar reasons, the electron and ion temperatures are not very different. The ion–electron equilibration time, τ_{ei}, ranges from 2 ms near the plasma edge to 10 ms in the core. These values are much less than the energy confinement time.

3. H MODES IN C-MOD OBSERVATIONS

Figure 1 shows traces from a typical ELM-free H mode, obtained after a short dithering period which

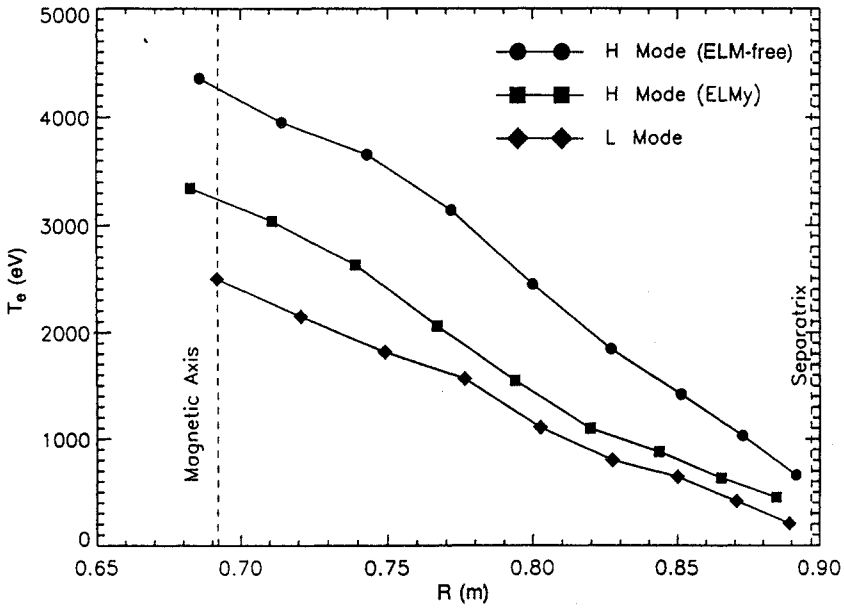

FIG. 3. Temperature profiles from L mode (shot 960130027), ELMy H mode (shot 960116010) and ELM-free H mode (shot 960116024). These shots all have $n_e = 3 \times 10^{20}$ m^{-3}, $P_{tot} = 3$ MW and $I_p = 1$ MA. The L mode discharge was obtained by running with reversed field, i.e. the ∇B drift was away from the divertor. This shot had confinement enhanced somewhat above that of ITER89 (~1.3), while the particular ELMy H mode shot shown had an H_{ITER89} factor near 1.8. The calculated separatrix positions for all three shots are the same, 0.896 m. The estimated error in the separatrix position is 0.002 to 0.003 m.

occurs as the ICRF power rises. This discharge had a plasma current of 1.0 MA, a toroidal field of 5.3 T and an elongation of 1.65; the safety factor at the 95% flux surface q_{95} was 3.7 during the H phase. There is no appreciable auxiliary heated L phase in this discharge as the ohmic input power, by itself, is very close to the threshold. In fact, L–H dithers can be seen during the ohmic phase at 0.67 to 0.69 s. Once the plasma enters H mode, strong increases are seen in density, stored energy and confinement time, $\tau_E = W_p/(P_{tot} - dW_p/dt)$. While the plasma density continues to ramp up during the entire H phase, the confinement enhancement, H_{ITER89}, [13] reaches 2.4 then drops gradually as the radiated power increases. Stored energy also dips slightly before the end of the RF pulse for the same reason. During the RF pulse, as the H mode develops, f_{rad} increases from about 0.20 to 0.75. The increase in radiated power is attributed to a dramatic increase in impurity confinement, which will be discussed in a later section. β_N reaches 1.5, which, while finite, is below the expected β limit, which is calculated to be in the range 2.0 to 3.0. Since the machine is running at high field, this β corresponds to very high pressures; central values of 0.5 MPa are regularly attained. The strong sawteeth seen on the electron temperature are common for all RF heating discharges, whether in L mode or H mode. The sawteeth, which are not seen on the ion temperature signal because of spatial and temporal averaging, only redistribute particles and energy in the plasma core and make a negligible contribution to global transport.

Under similar conditions, but at a slightly higher target density, ELMy H modes are obtained (Fig. 2(a)). After an initial drop, the H_α light increases and eventually exceeds the L mode levels. Most of this light originates in a high density, low temperature 'radiative condensation' region [14] located above the divertor 'nose' on the inner wall of the vacuum vessel. On top of this steady H_α light, numerous sharp spikes can be seen. These are signatures of ELMs, which come in clusters and are somewhat correlated with sawteeth. In this case, the plasma density rise is initially faster, but saturates and remains essentially constant during the rest of the H phase. Energy confinement is not quite as

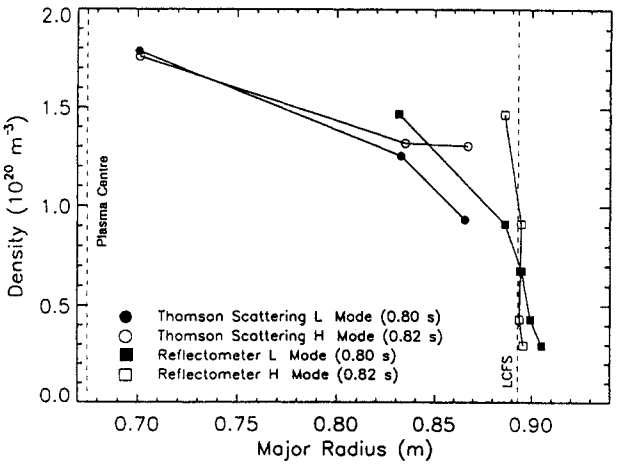

FIG. 4. Density profiles from L and H modes demonstrating an edge pedestal. For this shot $P_{tot} = 3.2$ MW and $I_p = 1$ MA.

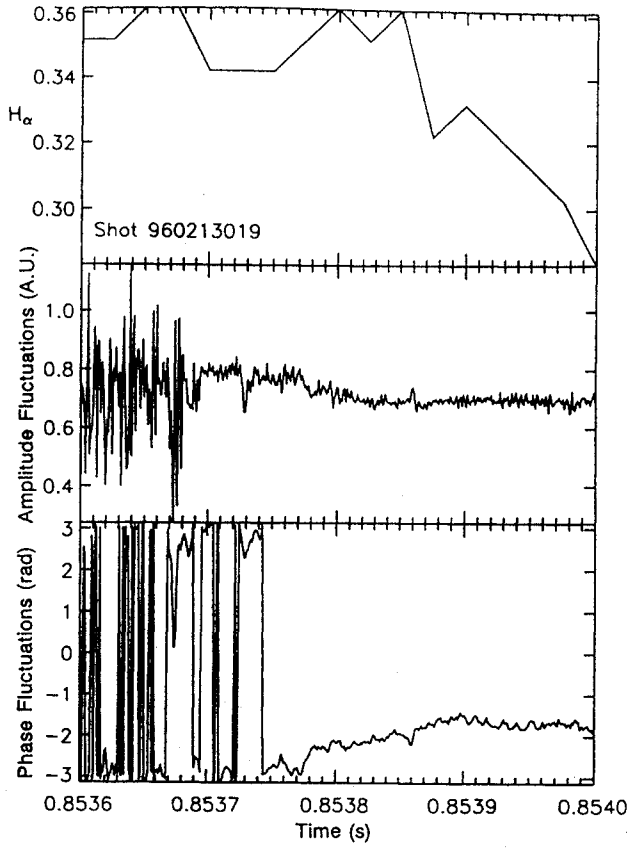

FIG. 5. Drop in edge fluctuations at L–H transition from reflectometry measurements at 88 GHz. The fluctuations drop in less than 100 μs following the transition. The shift in observation location, which accompanies the H mode density rise, is negligible for these short time intervals. This shot had a target density of $n_e = 1.8 \times 10^{20}$ m^{-3}, $P_{tot} = 3$ MW and $I_p = 1.2$ MA.

good as in the ELM-free discharge, H_{ITER89} reaching 2.0 and remaining at that level. Radiated power is lower for the ELMy discharge, $f_{rad} < 0.3$ for the entire H phase. As we will discuss later, the impurity confinement for these discharges, while substantially higher than for L mode, is well below the levels of the ELM-free discharges. Figure 2(b) shows an expanded view of several traces for the same shot. Details of the ELMs can be seen in the H_α and the edge electron temperature which is measured via ECE. Some admixture of density perturbation may be present in the ECE signal as the second harmonic emission is almost cut off at these densities. None the less, the perturbations are 'edge localized' and associated with a smaller average temperature pedestal, reduced impurity accumulation and slightly reduced energy confinement.

As seen on many other devices [15–17], the H mode transition is accompanied by a strong increase in the edge temperature and density. Figure 3 shows temperature profiles, taken with an ECE grating polychromator, comparing L and H modes with similar line averaged density, plasma current and input power. Data from outside the separatrix are available from fast scanning probe measurements [18]. The resolution for the ECE measurement is about 1 cm and the combined errors in measurement and separatrix position are about 0.3 to 0.5 cm, thus we cannot yet resolve the width of the transport barrier. Similar data are shown in Fig. 4, where density profiles from Thomson scattering and reflectometry are plotted before and after an L–H transition. The sharp edge gradients characteristic of the H mode transport barrier are clear, but instrumental resolution and positional uncertainties again limit resolution to about 1 cm. The reflectometry measurements also reveal that the transition is accompanied by a sharp drop in edge density fluctuations (Fig. 5). The decrease in fluctuations is always fast, typically occurring in less than 100 ms. The combination of strong edge gradients in temperature and density leads of course to a similarly strong edge pressure gradient. Even though the toroidal field is large, the edge β gradient, β', is substantial. The parameter $a = R\beta'$ reaches values of at least 0.4 and stability analysis shows many discharges with edge gradients at or above the ideal first stability limit. Nevertheless, no type I (giant) ELMs are observed [19]. Future work in this area will concentrate on improving the resolution of the edge profile measurements.

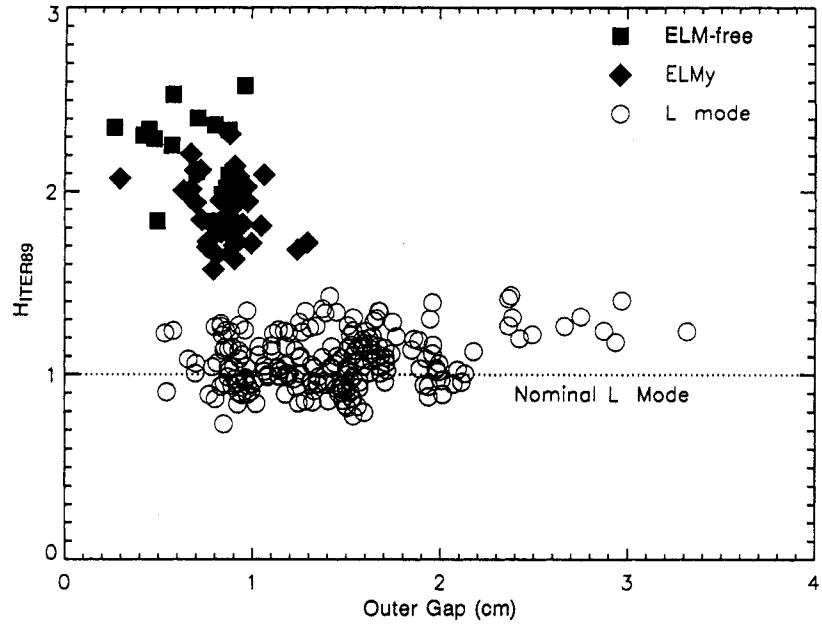

FIG. 6. Energy confinement enhancement versus outer gap. The estimated error for determining the separatrix position is 2 to 3 mm.

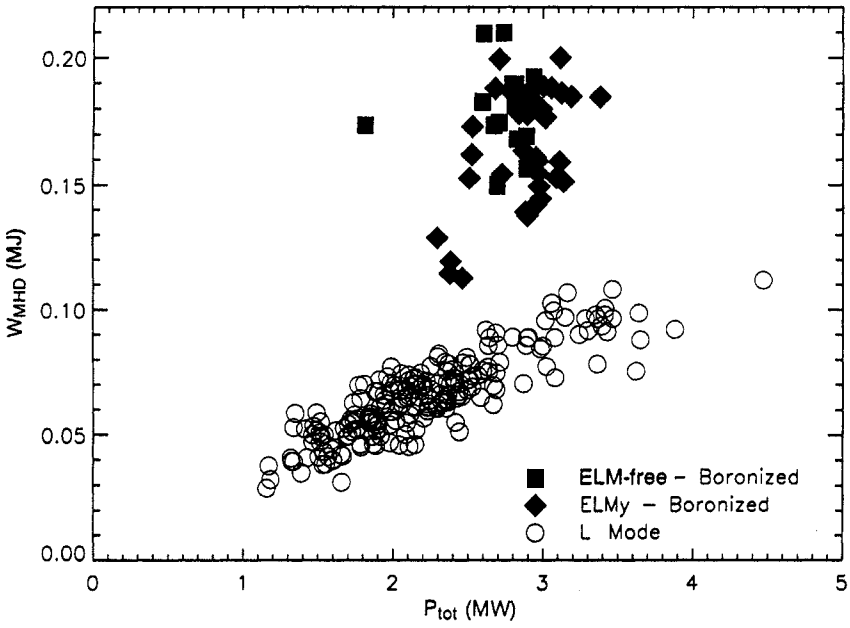

FIG. 7. Plasma stored energy versus total input power (P_{tot}) for L and H modes.

Profiles in the scrape-off layer (SOL) outside the separatrix are also altered during the H mode [3]. These profiles cannot be characterized by a simple scrape-off length in either L or H modes. Rather, the gradients are principally a function of local temperature; steepest near the separatrix, where the temperatures are highest, and flatter as one moves out from the separatrix, where the temperature is low. Following the L to H transition, the density and pressure scale lengths, near the separatrix, drop by about a factor of 2 to 2 mm and 1 mm, respectively; the latter value being roughly equal to the

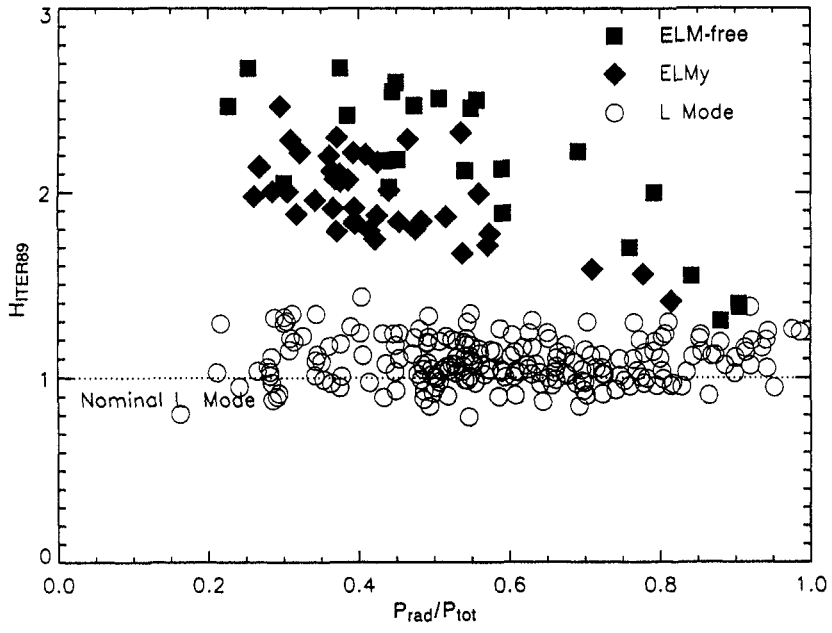

FIG. 8. H_{ITER89} versus P_{rad}/P_{tot} for L and H modes (H modes are for boronized discharges only).

local poloidal ion gyroradius. Temperature gradients are not as strongly affected and the temperature at the separatrix is approximately the same for L and H modes. The implication of these measurements is that the H mode transport barrier extends a short distance into the SOL. A side effect of these very sharp density gradients is the necessity of moving the plasma closer to the ICRF antenna, at the L–H transition, in order to maintain ICRF antenna loading. As shown in Fig. 6, this does not result in any degradation in confinement even with a gap between the separatrix and a nominal outer limiting surface of 2 to 3 mm. (The estimated error for determining the separatrix position is also about 2 to 3 mm.)

4. CONFINEMENT RESULTS

The improvement in energy confinement between L and H mode discharges can be clearly seen in Fig. 7, where the plasma stored energy is plotted versus input power. While there is more scatter in the H mode data, ELM-free H modes have on average 2.2 times the stored energy of the L modes. The corresponding ratio for ELMy plasmas is about 2. Figure 8 shows the confinement enhancement plotted against the radiated power fraction. This plot includes time slices with high radiated power that are excluded from the confinement database. Above $f_{rad} \sim 0.5$, H mode confinement degrades, approaching the L mode values as f_{rad} approaches 1.0. Remarkably, the global L mode confinement is unchanged over a range in f_{rad} from 0.2 to 1.0, showing an essential difference between L and H mode confinement. At the moderately high temperatures of these discharges, radiation is peaked in the edge region. While this has little effect on L mode plasmas, which already have a cool edge, it is devastating to the H modes, which require a much hotter boundary. This result may explain, in part, the improvement in performance seen in H modes with boronized walls. Figure 9 compares traces from ELMy H modes with similar plasma current, density and RF power taken before and after the boronization. The dramatic differences in radiated power, edge temperature and confinement enhancement are clear. Profiles of the radiated power for the two shots are shown in Fig. 10, indicating strong core radiation from molybdenum for the unboronized discharge. The effect on confinement can be seen in Fig. 11 where a comparison of the recent H mode data, obtained with boronized walls, and older data, obtained with bare molybdenum walls, [4] is shown. The older data have systematically higher radiated power and lower confinement;

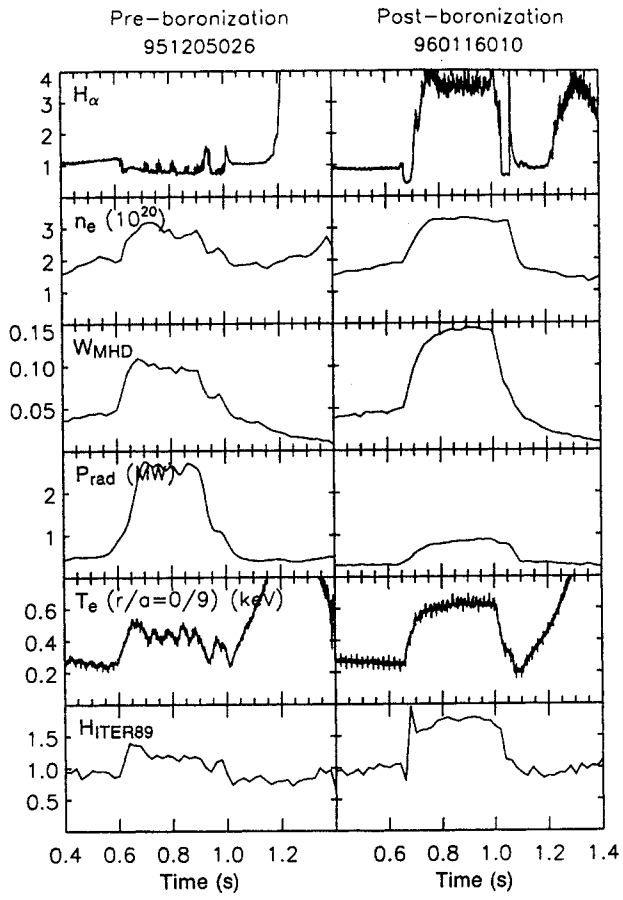

FIG. 9. Comparison of H modes with boronized and unboronized walls. Note the dramatic difference in radiated power and confinement enhancement. The apparent increase in edge T_e seen after 1 s is an artefact of the toroidal field rampdown.

however, this does not seem to be the only difference between the two sets of data, as the unboronized shots lie below the boronized ones for corresponding values of f_{rad}. High values of H were also obtained for unboronized ohmic H modes (which are not shown in the figure).

5. GLOBAL SCALING

So far we have discussed our H modes in relation to L modes and to L mode scaling. The parameter range for our H modes is not yet sufficient to reveal significant scaling trends in these data by itself; however, some features are worth discussing. The L mode data on C-Mod are consistent with ITER89-P, but a regression on the data yields a scaling that is much more 'Goldston-like' [20, 21] in its parametric dependence, $\tau_E \sim I_p/P^{1/2}$, although with a coefficient about 50% larger than that in Ref. [21]. The new H mode data are consistent with a multiplier of about 2 compared with our own L mode scaling. Although we have no data below $q_{95} \sim 3$ where confinement degradation has been reported [8], there is no clear dependence of the H mode enhancement over a range in q_{95} from 3 to 5. This can be seen in Figs 12(a, b) where the H factor (relative to H mode scaling laws) is plotted versus q_{95}. Here, we are concerned only with the trend versus q_{95}; the discrepancies with the scaling laws will be discussed in the next section. As seen on other machines [15], the best H modes have confinement times that approach, but do not exceed, values from ohmic, neo-Alcator scaling [22].

An obvious question is how C-Mod data compare with scaling laws previously derived from other machines. The ITER database group has assembled a large data set from a number of tokamaks and carried out systematic scaling studies [9]. Regressions are available for ELM-free and ELMy discharges and for total and thermal stored energy. We note at the outset that for C-Mod parameters, the thermal energy, calculated from these regressions, exceeds the total energy; an obvious impossibility. Figure 12(a) shows C-Mod ELM-free data compared with the corresponding ITER ELM-free H mode scaling law for total energy,

$$\tau_E = 0.048 I_p^{0.87} B_T^{0.45} m_{eff}^{0.43} R^{1.84} n_e^{0.03} \times \epsilon^{-0.02} \kappa^{0.53} P_L^{-0.55},$$

where the units are I_p in megamps, B_T in teslas, R in metres, n_e in 10^{20} m^{-3} and $P_L = P_{tot} - dW/dt$ in megawatts. In this case the H_H factor refers to enhancement above the nominal H mode scaling so that $H_H = 1$ corresponds to a match between the data and the scaling law. The C-Mod data are systematically above the $H_H = 1$ line, indicating better than predicted results. Figure 12(b) is a similar plot for ELMy data where the ITERH92-P(ELMy) scaling predicts [23]

$$\tau_E = 0.068 I_p^{0.9} B_T^{0.05} m_{eff}^{0.4} R^{2.1} n_e^{0.3} \epsilon^{0.2} \kappa^{0.8} P_L^{-0.65}.$$

In this case, the C-Mod data average about twice the predicted value. A possible culprit is the large size dependence seen in the scaling law. Also plotted on this figure is a comparison between the data and another commonly used expression to predict energy confinement for ELMy H modes, namely 0.85 times the ELM-free expression. While this is an improvement over the ELMy law, it underestimates the

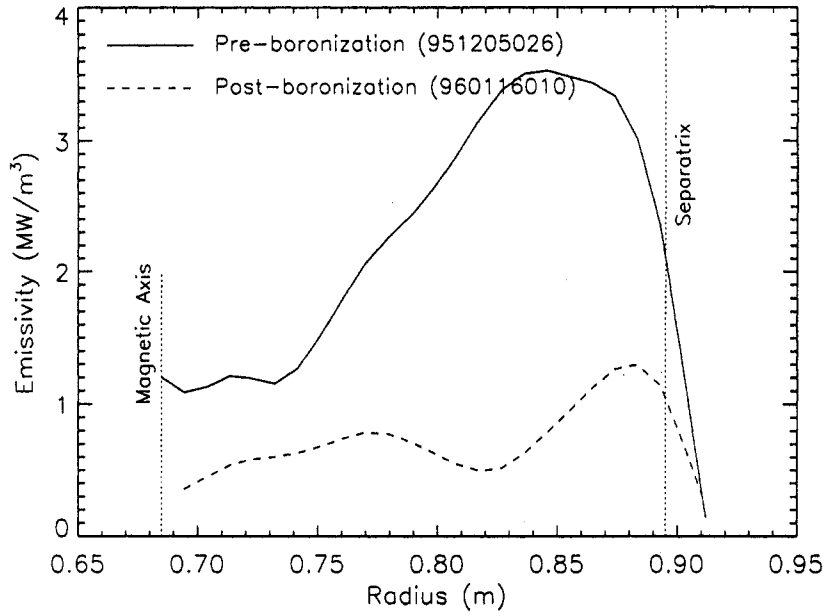

FIG. 10. Radiated power profiles for the two shots shown in Fig. 9.

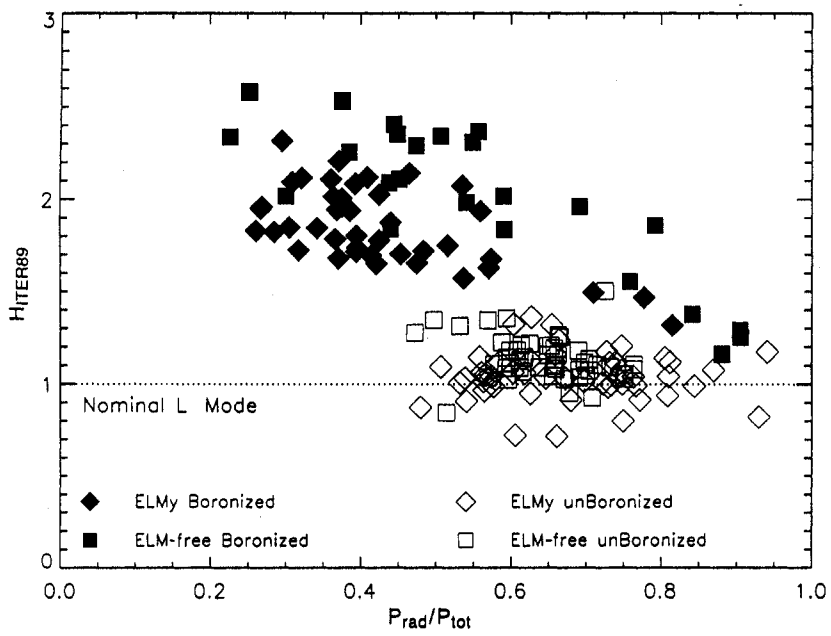

FIG. 11. H_{ITER89} versus $P_{\mathrm{rad}}/P_{\mathrm{tot}}$ for boronized and unboronized H modes.

C-Mod data by factors of 1.0 to 1.6. Another interesting exercise is to make a comparison with the scaling derived from controlled experiments on JET and DIII-D [24], two machines with plasma shapes similar to C-Mod. In this case, a scaling for ELM-free H modes, with dependences on P_{L}, I_{p}, which are evident from the individual data sets, and a scaling for R determined by a comparison between the machines, was reported. The authors also derived possible dependences on n_{e} and B_{T} from dimensional arguments. In this case, unique coefficients for n_{e} and B_{T} were not obtained, but instead, an equation relating the coefficient was derived consistent with the dimensionless, high-β constraint. Two possible sets of coefficients were calculated in Ref. [24], chosen to bracket dependences seen in other data. The results of

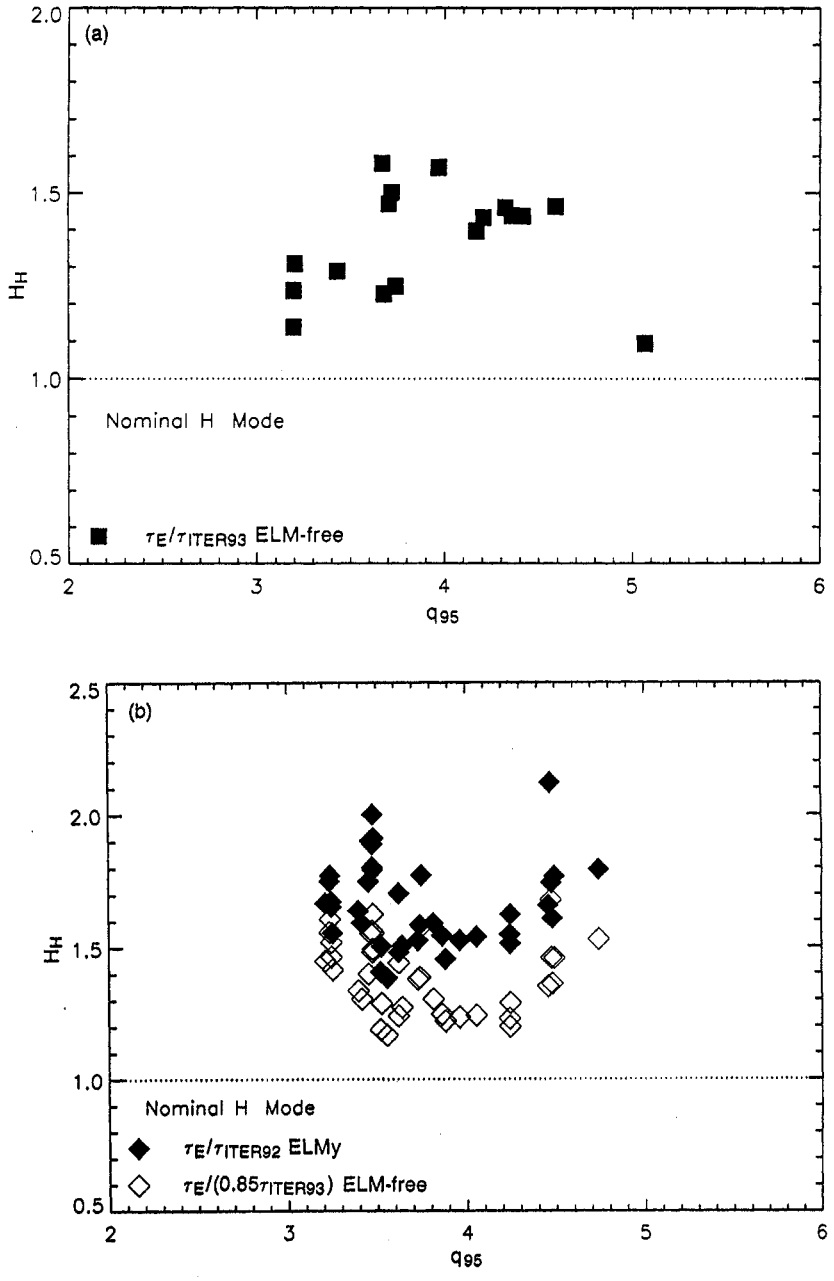

FIG. 12. (a) H_{ITER94} versus q_{95} for ELM-free data. (b) H_{ITER92} versus q_{95} for ELMy data.

a comparison between these results and C-Mod data are shown in Fig. 13. The standard JET–DIII-D scaling law, $\tau_E = 0.106 I_p^{1.03} R^{1.48} P_L^{-0.46}$, underestimates the C-Mod results by a factor of 1.7. This is not necessarily surprising because C-Mod was not run at the same B_T and n_e as the JET and DIII-D data. Of the extended scaling laws, with n_e and B_T included, the first, with a substantial B_T dependence, fails to fit the C-Mod data by the same margin as the unextended law. The second extension, with very weak n_e and B_T scalings but with less size dependence,

$$\tau_E = 0.14 I_p^{1.06} R^{1.4} P_L^{-0.45} B_T^{0.06} n_e^{0.07}$$

is much closer to the C-Mod data. As with the ITER scaling laws, our data suggest that the size scaling of the nominal JET–DIII-D law may be too strong.

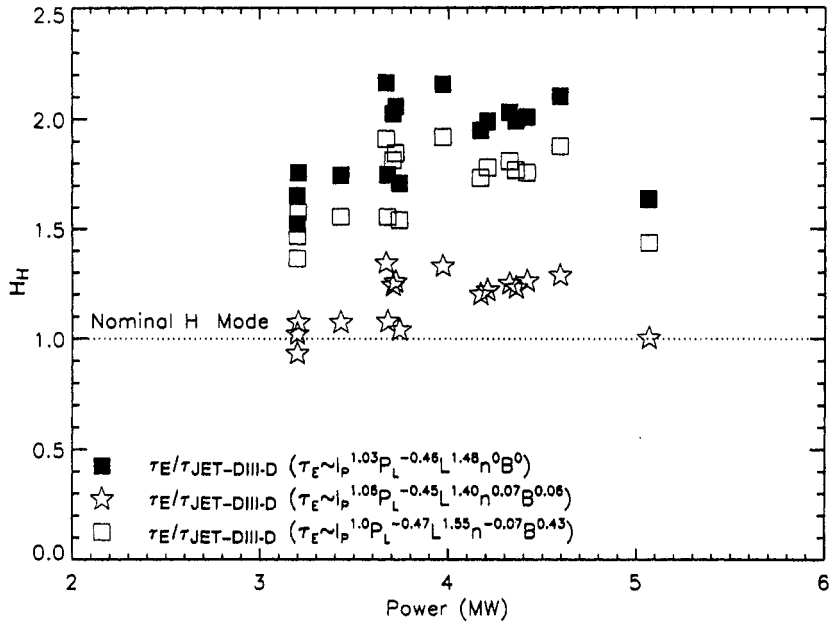

FIG. 13. $H_{\text{JET-DIII-D}}$ for all three versions of scaling law.

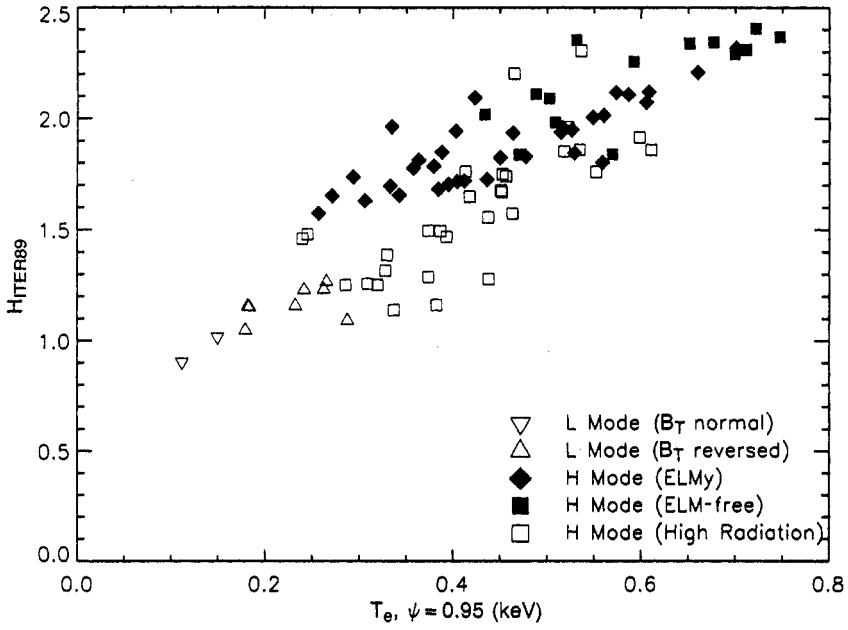

FIG. 14. H_{ITER89} versus edge temperature pedestal $T_e(\psi = 0.95)$.

6. TEMPERATURE PEDESTAL AND CORE TRANSPORT

The most salient feature of H mode plasmas is the edge temperature pedestal, which on C-Mod can vary from 0.25 to 0.8 keV. Not surprisingly, the largest pedestals tend to occur in ELM-free discharges with low radiated power; the smallest pedestals are correlated with ELMy or radiative discharges. Quantitatively, there is a clear correlation between the quality of confinement in H mode and the height of the edge pedestal. In Fig. 14, H_{ITER89} is plotted versus the electron temperature measured at the 95% flux surface. There appears to be an offset linear relationship between the H factor and the edge temperature; a trend that also fits a small set of L mode

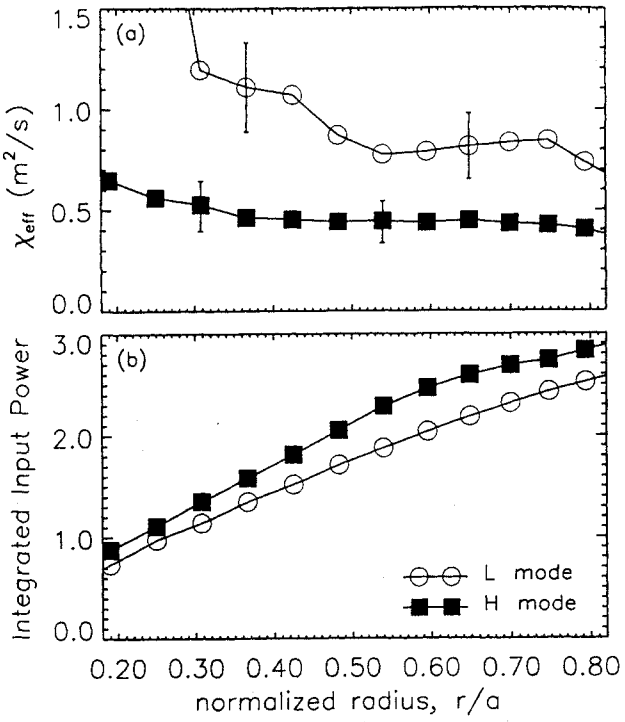

FIG. 15. (a) χ_{eff} versus r/a for L and H modes. (b) The integrated power density for these same discharges.

data, which is also shown. The L mode data are chosen to have engineering parameters as close as possible to those of the H modes. While the edge pedestal, by itself, can account for a part of the stored energy increase seen in H mode, a significant improvement in core confinement is also observed [15]. Figure 15 shows profiles of thermal diffusivity, comparing an H mode discharge with an L mode discharge for similar global parameters. At the densities present in these discharges, the measurements of the T_e and T_i profiles are not accurate enough to separate out the transport channels. Instead, we have plotted χ_{eff} defined by

$$\chi_{eff} \equiv (q_i + q_e)/(n_e \partial T_e/\partial r + n_i \partial T_i/\partial r).$$

What is found for these discharges and other similar pairs is that the diffusivity in H mode plasmas is about a factor of 2 lower than that in L mode plasmas, across most of the profile. Measurements in the SOL also show $\chi_\perp$ dropping by about a factor of 2 over a distance of 2 to 3 mm from the separatrix [3]. This implies that the transport barrier extends a few ion poloidal gyroradii into the scrape-off plasma.

Another interesting feature, seen in our data, is the relationship between the quality of the edge

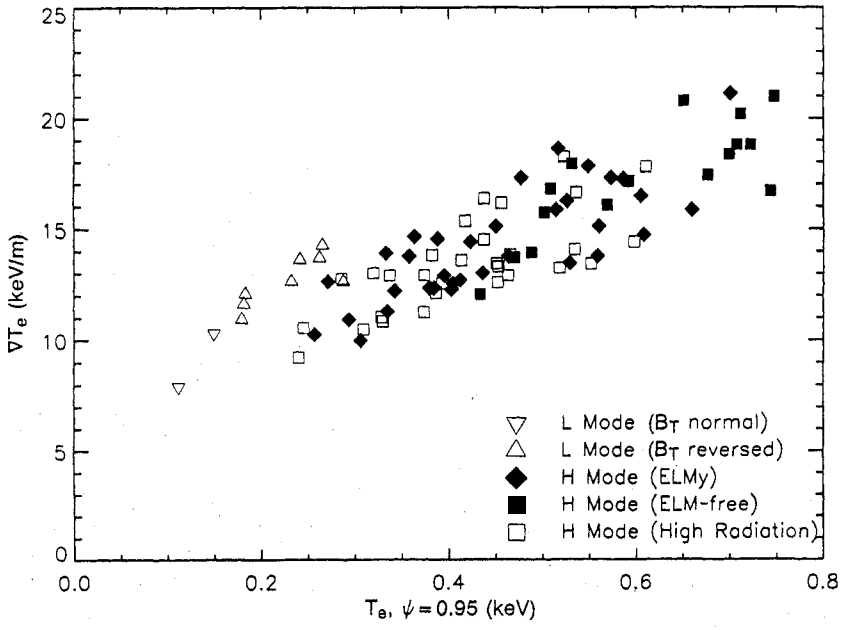

FIG. 16. ∇T_e in core versus $T_e(\psi = 0.95)$. The gradient is a spatial average taken between the outer edge of the sawtooth region and the beginning of the transport barrier.

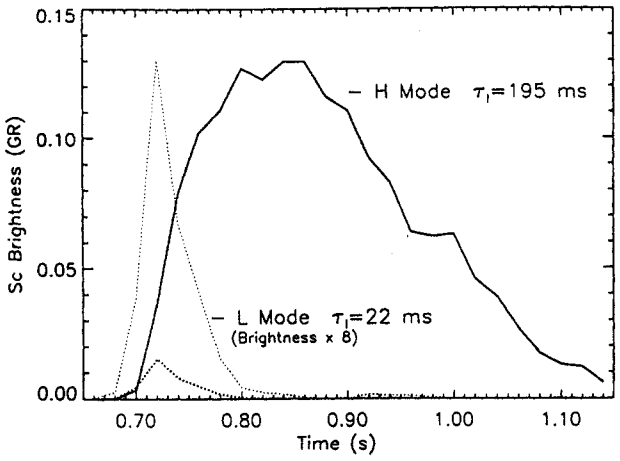

FIG. 17. Helium-like scandium radiation brightness (in GR = 10^{15} photons $\cdot$ cm^{-2} $\cdot$ s^{-1}) after laser blow-off for L and H modes. The L mode brightnesses are also shown scaled by a factor of 8 to make the difference between the two decays easier to see. For these shots $n_e = 3.2 \times 10^{20}$ m^{-3}, $P_{tot} = 2.9$ MW and $I_p = 1$ MA.

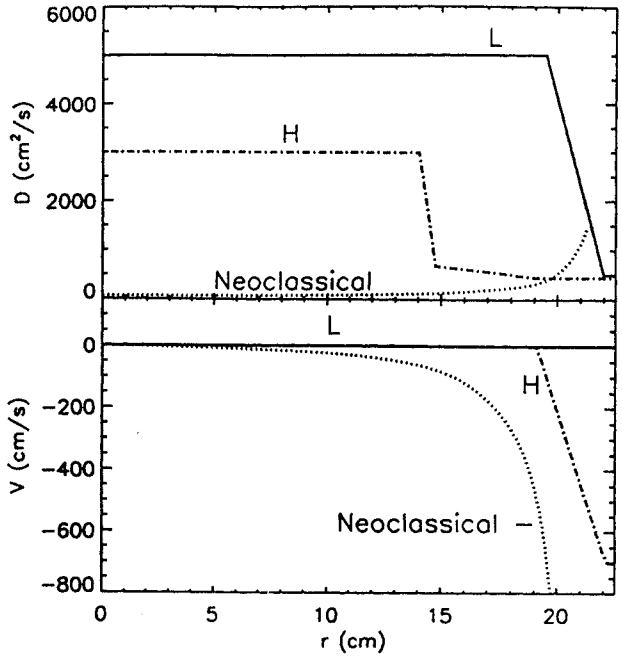

FIG. 18. Particle transport coefficients, D and V, from impurity injection data. The conditions are the same as those for Fig. 17.

transport barrier and the improvement in core transport. Figure 3 shows temperature profiles from L mode, ELMy H mode and ELM-free H mode discharges. Two trends are obvious:

(a) The discharges with the highest temperature pedestals have the best global confinement (as previously discussed) and

(b) The discharges with the best confinement also have the highest temperatures gradients in the plasma core.

This point is made again in Fig. 16, where the core temperature gradient is plotted against the edge pedestal height. The data show an offset linear relationship between the edge temperature and the core temperature gradient. Such a simple relationship raises the question about the role of marginal stability or critical gradients in determining plasma transport.

7. IMPURITY TRANSPORT

The increase in impurity levels that was discussed in an earlier section is not due to an increase in impurity source levels or to an improvement in impurity penetration. Impurity screening experiments indicate that the fractional penetration of injected gaseous impurities is lower in H mode than in L mode. Instead, the important factor in raising impurity levels is a dramatic increase in impurity confinement [25–27]. This phenomenon can be investigated by following the transport of trace amounts of non-intrinsic, non-recycling impurities that are injected into the plasma by the laser blow-off technique [28]. Figure 17 shows examples where scandium was injected into L and ELMy H mode plasmas. Brightness profiles of the lines from helium-like and lithium-like scandium were measured with an array of high resolution X ray spectrometers (HIREX [29]) and a scanning XUV grazing incidence spectrometer [30]. The helium-like scandium exists in the plasma core, while the lithium-like scandium is peaked at $r/a \sim 0.8$. Two important features of these experiments are evident; the decay times for impurities, τ_I, in the H mode plasmas are much longer than those in L mode; and the amounts of impurities that find their way to the plasma core are much greater. Impurity confinement times in ELMy H mode are at least 0.2 s, compared with ~0.02 s in L mode. This ratio is much larger than the corresponding ratio for energy confinement times; in H mode, τ_I is at least $3\tau_E$. During ELM-free discharges the impurity confinement can be even longer, so long that an accurate measurement is not possible. We estimate that $\tau_I > 0.5$ s for these cases.

Because spatial and temporal data are available from the measurements, it is possible to compare the

measurements with transport simulations using the MIST code [31, 32], where the transport is modelled as $\Gamma = -D(r)\nabla n_I + V(r)n_I$. While this approach does not necessarily produce a unique solution for the transport coefficients, it does demonstrate essential features that these coefficients must have. To account for the long decay time, the diffusion coefficient must be substantially lower in H mode plasmas, while the increase in impurity inventory can be explained by a strong inward pinch, localized in the plasma edge. An example of transport coefficients that can produce a good match to the data is shown in Fig. 18. These results are similar to those reported on DIII-D [33], although these transport coefficients are substantially larger than the ones shown here for C-Mod. It is also worth noting the similarity in magnitude between the diffusion coefficients shown here and the thermal diffusivity shown in Fig. 15. The two sets of curves are of the same magnitude and the reduction in diffusivity seen at the L–H transition is about a factor of 2 in both cases. There is no analogy to the very strong inward pinch seen in the particle transport and this accounts for the very different values for particle and energy global confinement.

8. SUMMARY AND DISCUSSION

We have reported on energy and impurity particle confinement in ELMy and ELM-free H modes in a high field, high density regime. The beneficial effects of boronization were demonstrated once again; plasmas run on boronized walls had better confinement and lower radiated power than those run on untreated molybdenum walls. It is important to note that the surface power densities in C-Mod exceed those of all other tokamaks, reaching values predicted for ITER or other burning plasma devices. With boronization, confinement enhancements over 2 were routinely obtained for a period of many confinement times. Quasi-steady conditions were reached in ELMy, enhanced recycling discharges. Energy and particle diffusivities were found to be of the same magnitude and each decreases by approximately a factor of 2 after an L–H transition. The difference, the global impurity confinement being many times longer than the energy confinement in H mode, is attributed to a strong inward particle pinch at the discharge periphery. We have found a clear linear relationship between the edge pedestal temperature and the core temperature gradient. This behaviour is consistent with critical gradient models (e.g., ion temperature gradient theories), but confirmation awaits quantitative comparisons.

In our studies of H mode plasmas, we have measured energy confinement times that are consistently higher than what is predicted by the commonly used scaling laws. These scaling laws, which have a 10 to 20% root mean square error about the data that were used to derive them, did not reference C-Mod data; thus, our experiments provide an excellent test for extrapolation of these laws. The result, that C-Mod data lie outside the fitting errors, should call into question the use of these laws for extrapolation. In particular, attention needs to be paid to scaling law dependences that are not readily apparent in data from individual machines. In this case, data covariances that occur naturally may be corrupting the results. For example, τ_E is usually seen to have only a weak dependence on n_e or B_T [8, 25]; however, n, B_T and R have a natural covariance through the density limit that scales roughly as B/R and could result in incorrect fitting coefficients for all three variables. In particular, our data may suggest that the size scaling in the scaling laws is too strong. Other variables, for example, divertor compression and neutral pressure (which are very high in C-Mod), may be important for H mode confinement, and have not yet been included in empirical scaling laws. Of course, in the absence of a comprehensive first principles theory for plasma transport, empirical scaling will remain an essential tool, but we must constantly remind ourselves of the limitations of that approach.

ACKNOWLEDGEMENTS

The authors wish to thank the rest of the Alcator team, the technical staff, engineers, students and scientists whose hard work keeps the machine running and productive. This work was supported by USDOE Contract No. DE-AC02-78ET51013.

REFERENCES

[1] HUTCHINSON, I.H., et al., Phys. Plasmas **1** (1994) 1511.
[2] LIPSCHULTZ, B., et al., J. Nucl. Mater. (in press).
[3] LaBOMBARD, B., et al., Experimental investigation of transport phenomena in the scrape-off layer and divertor, J. Nucl. Mater. (in press).

[4] SNIPES, J.A., et al., Phys. Plasmas **3** (1996) 1992.
[5] SCHNEIDER, U., et al., J. Nucl. Mater. **176&177** (1990) 311.
JACKSON, G.L., et al., Phys. Fluids B **4** (1992) 2181.
[6] WINTER, J., et al., J. Nucl. Mater. **162–164** (1989) 713.
[7] LAO, L., ST. JOHN, H., STAMBAUGH, R., KELLMAN, A., PFEIFFER, W., Nucl. Fusion **25** (1985) 1611.
[8] CHRISTIANSEN, J.P., et al., Nucl. Fusion **32** (1992) 291.
[9] ITER H MODE DATABASE WORKING GROUP, Nucl. Fusion **34** (1994) 131.
[10] HAWRYLUK, R.J., in Physics of Plasmas Close to Thermonuclear Conditions (Proc. Course Varenna, 1979), Vol. 1, CEC, Brussels (1980) 19.
[11] SMITHE, D., COLESTOCK, P., KASHUBA, R., KAMMASH, T., Nucl. Fusion **27** (1987) 1319.
[12] HAMMET, G., Fast Ion Studies of Ion Cyclotron Heating in the PLT Tokamak, PhD Thesis, Princeton Univ., NJ (1986).
[13] YUSHMANOV, P., et al., Nucl. Fusion **30** (1990) 1999.
[14] LIPSCHULTZ, B., et al., Nucl. Fusion **24** (1984) 977.
[15] WAGNER, F., et al., Phys. Rev. Lett. **49** (1982) 1408.
[16] KAYE, S.M., et al., J. Nucl. Mater. **121** (1984) 115.
[17] JAHNS, G.L., GROEBNER, R.J., ST. JOHN, H., Nucl. Fusion **29** (1989) 1271.
ASDEX TEAM, Nucl. Fusion **29** (1989) 1959.
[18] LaBOMBARD, B., et al., Phys. Plasmas **2** (1995) 2242.
[19] ZOHM, H., Plasma Phys. Control. Fusion **38** (1996) 1213.
[20] GREENWALD, M., et al., Phys. Plasmas **2** (1995) 2305.
[21] GOLDSTON, R.J., Plasma Phys. Control. Fusion **26** (1984) 87.
[22] PARKER, R.R., et al., Nucl. Fusion **25** (1985) 1127.
[23] ITER H MODE DATABASE WORKING GROUP, in Plasma Physics and Controlled Nuclear Fusion Research 1992 (Proc. 14th Int. Conf. Würzburg, 1992), Vol. 3, IAEA, Vienna (1993) 251.
[24] SCHISSEL, D.P., et al., Nucl. Fusion **31** (1991) 73.
[25] ASDEX TEAM, Nucl. Fusion **29** (1989) 1959.
[26] IDA, K., et al., Nucl. Fusion **29** (1989) 231.
[27] JET TEAM, in Plasma Physics and Controlled Nuclear Fusion Research 1990 (Proc. 13th Int. Conf. Washington, DC, 1990), Vol. 1, IAEA, Vienna (1991) 261.
[28] MARMAR, E.S., CECCHI, J.A., COHEN, S.A., Rev. Sci. Instrum. **46** (1975) 1149.
GRAF, M., Impurity Injection Experiments on the Alcator C-Mod Tokamak, PhD Thesis, Massachusetts Inst. of Technol., Cambridge, MA (1995).
[29] RICE, J.E., MARMAR, E.S., Rev. Sci. Instrum. **61** (1990) 2753.
[30] TERRY, J.L., MANNING, H.L., MARMAR, E.S., Proc. SPIE – Int. Soc. Opt. Eng. **689** (1986) 54.
[31] HULSE, R.A., Nucl. Technol. Fusion **3** (1983) 259.
[32] WANG, Ying, A Study of Impurity Screening in Alcator C-Mod Plasmas, PhD Thesis, Massachusetts Inst. of Technol., Cambridge, MA (1996).
[33] PERRY, M.E., et al., Nucl. Fusion **31** (1991) 1859.

(Manuscript received 29 August 1996
Final manuscript accepted 10 March 1997)

(E-mail address of M. Greenwald:
g@psfc.mit.edu)